Seeing through Murky Matter using Laser-induced Fluorescence

A thesis submitted in partial fulfillment of the requirement
for the degree of Bachelor of Science in
Physics from the College of William and Mary in Virginia,

by

Jenna M. Klotz

_____

Advisor: Professor William E. Cooke

Williamsburg, Virginia
May 2002

ABSTRACT

Current techniques used to image gene expression *in vivo* use invasive surgical procedures or harmful gamma rays to analyze tissue. Optical imaging of tissue is difficult because the majority of light is absorbed by tissue. In the near infrared (NIR) region, however, absorption of light decreases and it is possible to "see" through tissue. Though absorption is minimal in the near infrared region, scattering due to tissue heterogeneities hinders optical imaging. We are developing a detector for laser-induced fluorescence in the NIR using a modulated avalanche photodiode (APD) to amplify the signal and the time delay of fluorescence to differentiate between scattered light and fluorescence. We have shown that by modulating the avalanche photodiode, we can amplify the signal by nearly 70%.

Introduction

Gene therapy was envisioned to treat diseases caused by defective genes. In gene therapy, a different set of genes is introduced to replace the faulty genes. Monitoring the effects and progress of the treatment requires imaging the cells and genes *in vivo*.

The goal of molecular imaging is to survey cell biology, specifically gene expression, in its natural and living state, without causing harm to the cells. The primary method used for gene expression is tissue analysis.[1] Tissue analysis examines macroscopic physical, physiologic, and metabolic changes for tissue differentiation instead of identifying the DNA mutations or specific DNA sequences responsible. Furthermore, many *in vitro* analytic techniques that do focus on such genetic factors are either inapplicable or not as effective *in vivo*.

Current *in vitro* analytic techniques of genetic factors include the following: northern blot for RNA; southern blot for DNA; western blot and immunostaining for protein expression; polymerase chain reaction (PCR) and restriction fragment length polymorphism mapping (RFLP) for DNA fingerprinting; luminometers for luciferase marker gene detection; and enzyme staining for ß-galactosidase expression.[1] Though these techniques have many benefits *in vitro*, none are applicable *in vivo*.[2] Blots, by definition, are *in vitro* and require grinding of the DNA. Immunostaining, likewise, is performed *in vitro* by definition, as it requires that one remove tissue from the animal and place it on a slide. PCR requires thermal slicing of DNA sequences and centrifuges out DNA, destroying the cell in the process. RFLP uses enzymatic digestion of DNA to produce fragments, which are then separated by electrophoresis. In order for luminometers to be effective *in vivo*, the animal whose tissue is being analyzed must be small and transparent. Even worse is enzyme staining, which is only capable of analyzing dead tissue.

Some imaging techniques involve the introduction of radiolabeled antibodies1,[3] and viral and non-viral vectors1. *In vitro*, radiolabeled antibodies have proven useful in understanding and

imaging molecular components of cells. Unfortunately, when used in *in vivo* analysis, the efficacy of the radiolabeled antibodies noticeably decreases due to biological barriers like substantial uptake in the liver and poor penetration into tumors. The problem with radiolabeled viral and non-viral vectors is that they do not show that the protein of interest is being expressed; they merely indicate the location of the genetic delivery system. One particularly promising marker gene is Herpes Simplex Virus type 1 thymidine kinase (HSV-1-tk), which has been tested *in vivo* in mice, using gamma cameras, single photon emission computed tomography (SPECT), and positron emission tomography (PET1). Despite the success of HSV-1-tk in *in vivo* imaging in mice, the introduction of a transgenic organism in humans is simply not feasib2le.

Though other imaging techniques, such as magnetic resonance imaging (MRI) and *in vivo* microscopy, do not involve the introduction of a transgenic organism, they still have limits on their usefulness for imaging gene expression.1 MRI is capable of imaging structure, but not imaging specific genes. While MRI can be used to image gene delivery vectors, it images the delivery system, not the protein expressed2. MRI only images the gene delivery vector indirectly, requiring a magnetic contrast agent. This contrast agent is inefficient. The majority of it does not bind to any specific molecule. Consequently, MRI images what is injected into the tissue (the vector) and not protein expression. *In vivo* microscopy, on the other hand, has already successfully imaged gene expressio1n. *In vivo* microscopy uses a confocal lens to focus a laser beam at different layers within a tiss2ue. This method is only effective up to depths of 60 µm. To look at tissues deeper than 60 µm, doctors surgically open up the tissue, which is very invasive. Given the surgical manipulation, the tissue is not exactly *in vivo* as it is no longer in its natural state.

The 800 nm Window

The solution to these myriad problems of current imaging techniques is known as the 800 nm window. The imaging of tissues at depths of 500 µm to 1 cm requires the use of near infrared (NIR) light.3 Hemoglobin, the major absorber of visible light, has minimal light absorption above 650 nm. Water, the major absorber of infrared light, has minimal light absorption below 900 nm. This creates a 650-900 nm window, where the absorption coefficient of tissue is lowest. Between 700 and 900 nm, photon transport is dominated by scattering rather than absorption.[4] Increased scattering is the major drawback to imaging in the NIR. Advantages of NIR fluorescence include: a minimal amount of background signals; good precision and accuracy of lifetime measurements; and imaging in the NIR requires simpler instrumentation than other techniques. Studies using small peptide-coupled NIR fluorochromes in place of radiolabeled antibodies show promising results for imaging using NIR light.[3,5] These fluorochromes are less immunogenic and penetrate tissue better than antibodies. Furthermore, side effects occurred in less than 0.15% of the patients. "Inherently linked to the development of the described probes is the need to develop tomographic three-dimensional imaging systems that can accurately quantify NIR fluorochrome concentrations and fluorescence activation in deep heterogeneous media *in vivo*." [3] Optical imaging in the NIR has at least three benefits: it is non-invasiv5e; fluorochromes are less harmful to tissue than radiolabeled antibodi5es; and fluorescence is an efficient contrast age2nt.

Though the outlook for NIR imaging is promising, the large amount of scattered light hinders detection of fluorescence. To image laser-induced fluorescence, you must be able to separate fluorescence from scattered light. Using the time delay of fluorescence, it is possible to differentiate between scatter and fluorescence using phase sensitive techniques. Laser-induced fluorescence begins at the same time as the laser pulse exciting the tissue (see Figure 1). The

goal of our research is to detect laser-induced fluorescence in a turbid medium using wavelength

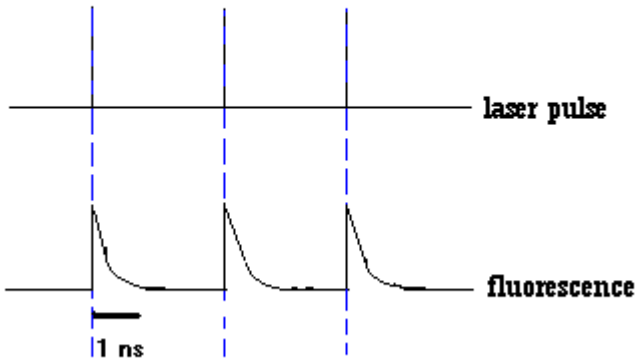

discrimination and the time delay of fluorescence.

Figure 1: The fluorescence pulse starts at the same time as the laser pulse. The blue dashed line marks the start of both the laser pulse and the fluorescence decay. The fluorescence decay signal lasts for approximately 1 ns.

Imaging in the NIR: Other approaches

Before beginning experimental work, it was first necessary to research recent approaches to imaging in the NIR. Three of the most relevant methods are time correlated single photon counting (TCSPC), and the use of diffuse photon density waves (DPDW) and fiber optic probes.

Time Correlated Single Photon Counting

Time correlated single photon counting collects data in the form of light intensity versus time.[6] "Bright" light contains more photons than "dim" light. Therefore, to measure intensity, one need only count. Fluorescence decay can be viewed as a pulse that starts out bright and then rapidly decays in intensity. In TCSPC, for a given fluorescence event, a single photon is captured or detected. For that photon, one measures the time elapsed between the arrival of the

excitation signal at the sample and the detection of the photon. The start time, t=0, is the time at which the sample is bombarded with the light energy that excites the sample and causes fluorescence. The laser used in this example was a GaAlAs diode laser with a pulse width of 150 ps and an average power of 5 mW. When the light source, such as a laser, sends a pulse to the sample, it simultaneously sends a start signal to a time to amplitude converter (TAC). When a single photon enters the detector, the detector sends a signal plus noise pulse to a stop discriminator. The stop discriminator is only active when the signal's amplitude falls within a designated range, usually determined by the noise level of the detector and the signal plus noise pulse. This active range allows the discriminator to eliminate the effects of the detector noise. When the stop discriminator receives a signal within this range, it sends a stop signal to the TAC. The TAC then generates a signal whose amplitude is equal to the time elapsed between the start and stop signals. For each photon, one count is added to the x-axis of a plot of intensity versus arrival time. The intensity scale of the plot actually represents the number of photons counted in the time slots shown on the x-axis. Millions of repeated measurements create a histogram, which eventually forms a curve representing fluorescence decay. Figure 2 shows the procedure by which photon counting creates a fluorescence decay curve.

The advantages of TCSPC are single photon sensitivity, favorable time resolution, and insensitivity to noise. Single photon sensitivity is beneficial because it improves the precision of the measurements, reducing the amount of lost data. Favorable time resolution in fluorescence decay measurements is important because fluorescence events can be picoseconds in length,[7,8] though strong fluorescent dyes usually have decay times on the order of 1 ns. Insensitivity to noise is important because it ensures that only the fluorescence decay signal is detected. The main disadvantage of TCSPC is that because only a single photon is captured for a given fluorescence event, we lose most of the data.

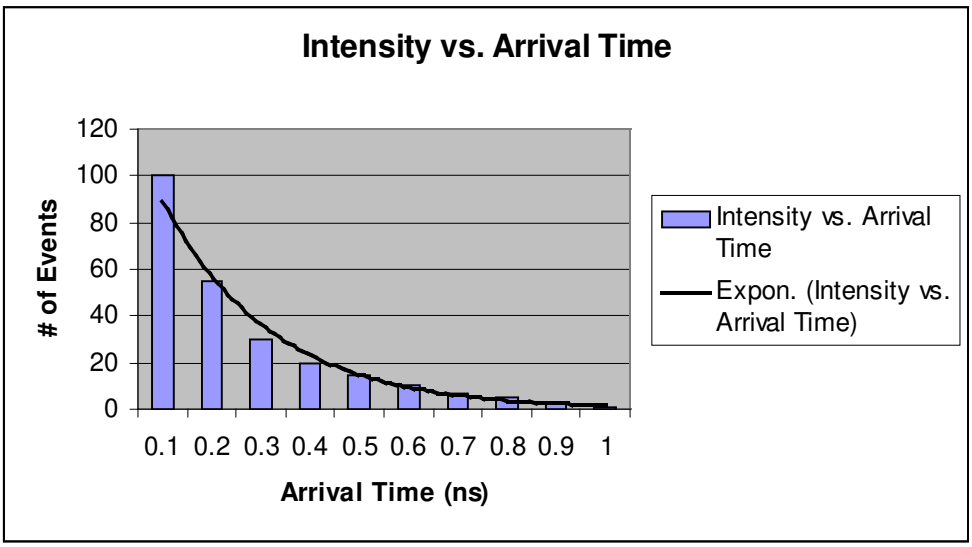

Figure 2: A plot of intensity vs. arrival time of photons detected using time correlated single photon counting, using simulated data. The y axis represents the number of photons that are detected in a time slot shown on the x axis. After millions of repeated measurements, the resulting histogram is representative of fluorescence decay. The black curve represents fluorescence decay.

Applications of TCSPC include NIR imaging of DNA microarrays,[7] base calling,[8] and DNA sequencing.8 For these applications, tricarbocyanine dyes are often used as probes. Tricarbocyanine dyes contain isothyocyanate and succinimidyl ester functional groups, which are reactive toward primary amines.[9] These dyes can therefore be used as probes for amino acids, the building blocks of proteins. All dyes containing these functional groups show absorption and emission maxima in the 770 to 810 nm region, and were shown to enhance fluorescence. Tricarbocyanine dyes require only one detection channel to process their fluorescence data because of their similar absorption and emission maxima. These dyes thus serve as excellent labels in methods using lifetime discrimination. Lifetime measurements, made by TCSPC, for example, have been proposed as an alternative to wavelength discrimination in the analysis of fluorescence in tissue.

Diffuse Photon Density Waves

Individual photons undergo a random walk within a medium, but when viewed collectively, a spherical wave of photon density is produced and propagates outward from the source.4 This is a diffuse photon density wave (DPDW). DPDWs exhibit the same properties as all light: refraction, diffraction, dispersion, interference, and scattering. To generate a DPDW, one typically sends an amplitude-modulated signal into a turbid medium via a source fiber optic cable, and then collects the photons using a detector fiber optic cable. One then uses standard phase sensitive methods to separate the oscillating light from the rest of the signal. This technique only produces DPDWs of a single frequency.

To study turbid media using DPDWs of multiple frequencies, there are three possible ways to generate the DPDW.[4] Though DPDWs generated by a continuous-wave source provide us with information about the sample, based on distortions of the constant-amplitude contours, the signal does not oscillate with time. Therefore, phase-sensitive methods of separation are useless. Using modulated disturbances to generate DPDWs provides us with phase information, but due to the large absorption factor of tissue, higher modulation frequencies do not improve the quality of the image produced by analyzing temporal changes of the DPDW. The best way to generate a DPDW is to use short light pulses. The pulse broadens as it moves through the medium. The scattering factor of the medium determines the peak time delay of the broadened pulse and the terminal slope of the pulse depends on the medium's absorption factor. A series of pulses can be treated as a superposition of DPDWs, each scattering independently. It is easy to analyze the series of pulses using standard time- or frequency-domain techniques.

Initial research testing the effectiveness of DPDW in NIR imaging studied DPDWs in Intralipid, which has similar optical properties to human tissue in the NIR region.[10] Researchers ran a source fiber cable through a fish tank, containing only Intralipid. Absorptive slices were

then added to the tank and the measurements were repeated. The researchers were able to accurately calculate the position of the slices and to produce a two-dimensional image of the shapes of the slices. To make a three-dimensional image, one could either repeat the experiment at a different depth or take another two-dimensional image from an orthogonal view. This technique has since progressed from imaging absorptive slices to imaging regions of the brain.[11] Near-infrared radiation penetrates the skull much better than ultrasound4. NIR can penetrate centimeters into the scalp, skull, dura, and brain11. The regional imager developed by Yodh et a11l. uses two intensity-modulated diode lasers that operate at 779 nm and 834 nm to produce DPDWs. The laser modulation frequency, the laser wavelength, and the optical properties of the tissue being examined determine the interactions between the DPDWs and the tissue. A pad, approximately 40 cm^2, containing 12 source fibers and 4 detector positions, is placed on the head in the region to be imaged. The pad produces two-dimensional images of the brain.

Fiber Optic Probes

The pigments of tissue reduce the intensity of light signals. Fluorescence is further affected by the long path length of travel in tissue, as well as by variation in blood flow and tissue heterogeneities. These factors combined are responsible for the multiple scattering of the excitation and fluorescent light. The majority of methods to measure tissue fluorescence use large core fiber bundles that permit the troublesome multiple scattering. An alternative technique is the development of a model of fluorescence light propagation in tissue. Two models are the diffusion theory and the Monte Carlo scattering model.[12] Diffusion theory is limited in its application because the tissue sample needs to be relatively large and homogeneous. The Monte Carlo scattering model describes light propagation in tissue with exact geometry, but requires that the tissue properties and layers be well understood. Yet another alternative approach is to

use small sample tissue volumes and confine the probed tissue region to a diameter smaller than the scattering length of tissue (100 µm in humans), thereby minimizing scattering and absorption.

The 1998 study by Pogue and Burke combined the Monte Carlo scattering model with this last approach. Researchers used Monte Carlo simulations as a theoretical comparison for their experimental results using fiber optic bundles. Preliminary experiments attempted to use a single fiber, but the low intensity of the fluorescent light made measurements difficult to obtain. This problem was solved by using a bundle, 1mm in diameter, of 30 fibers, each 100 µm in diameter spaced 500 µm apart. The bundle was tested in 1% Intralipid solution. This fiber optic probe was found to be insensitive to background absorptive molecules and detected fluorescence linearly proportional to fluorophore concentration. The bundle allows imaging of a region larger than the scattering length of human tissue, while maintaining localized sampling of regions smaller than the scattering length. Therefore the reduced scattering and absorption achieved by the small fibers are preserved. The fiber optic bundle provides a noninvasive, relatively inexpensive, and less time consuming approach to tissue imaging, compared to tissue extraction and radiolabeling. Using smaller fiber optics, however, limits the depth of tissue that can be analyzed. This technique may therefore be constrained to superficial tissue layers.

Evidence of Absorption and Laser-induced Fluorescence

Using a diode laser as an excitation source, we collected data on laser-induced fluorescence in weak samples of the dye LDS 821 in a glass cuvette (see Figure 3 for set up).

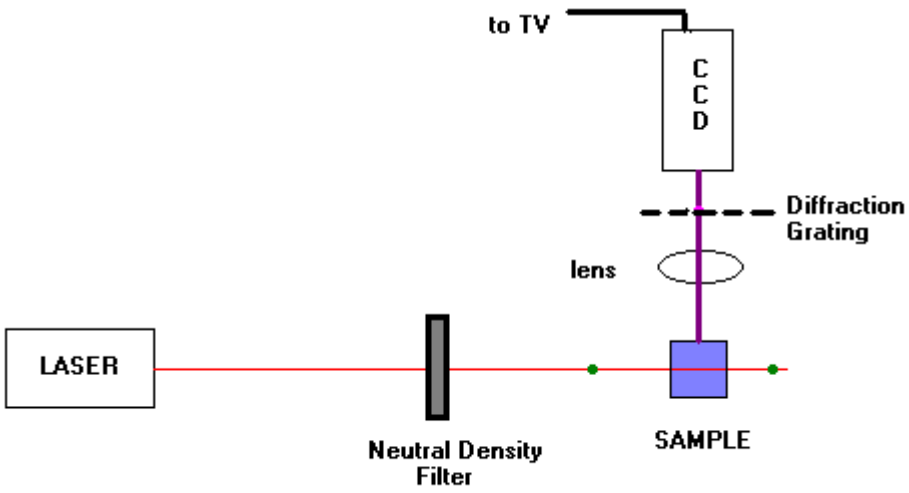

Figure 3: Set up to measure absorption and laser-induced fluorescence of weak samples of LDS 821-methanol solutions. The green dots mark the positions of the power meter. When we attenuated the laser, the attenuators were placed at the blue dot. The pink dot marks the position of the diffraction grating when we attempted to separate scatter and fluorescence.

LDS 821 has an absorption wavelength maximum of 574 nm and a fluorescence maximum of 750 nm. We measured the absorption of different concentrations of dye-methanol solutions using a power meter to measure the intensity of the beam before and after it passed through the solution (see Table 1). We qualitatively measured laser-induced fluorescence of each dye-methanol solution using a charged coupled device (CCD) camera and television (see Table 1). The CCD camera is capable of detecting fluorescence of dye solutions on the order of 10^{-6} M. Figure 4 shows an image of laser-induced fluorescence that we took using the CCD camera. Data indicated a positive correlation between dye concentration, absorption, and the intensity of the laser-induced fluorescence.

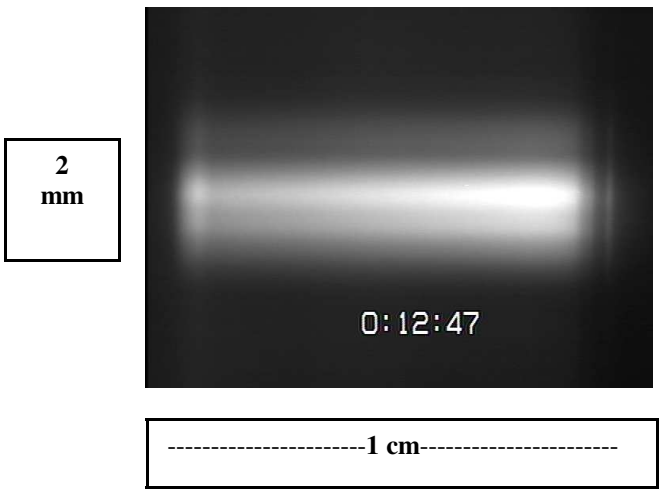

Figure 4: Image of laser-induced fluorescence of dye-methanol solution, concentration 2.4 x 10^{-5} M, taken by CCD camera.

To establish the relationship between the intensity of the laser, absorption, and the intensity of laser-induced fluorescence, we placed neutral density filters between the excitation beam and sample (concentration 3.9 x 10^{-5} M). We repeated the above procedure to measure absorption and fluorescence. Our data showed that higher intensity excitation light resulted in greater absorption and higher intensity laser-induced fluorescence (see Table 2).

Table 1: Power readings of laser before and after it passes through dye-methanol solution (path length = 1 cm) and television observations of laser-induced fluorescence at various concentrations of LDS 821.

Solution Concentration (10^{-6}M)	**Power of excitation source (mW)**	**Power of beam after passing through solution (mW)**	**Percent absorption**	**TV observations of LIF**
Empty cuvette	27.8	24.8	11	None
Methanol	28.1	26.5	6	None
97	26.4	9.3	65	Very visible
49	27.2	12.8	53	Very visible, elongated
24	27.2	16.8	38	Thinner, smoother edges, dimmer
12	28.3	20.7	27	Thinner, dimmer
6.1	27.9	21.9	22	Same as previous image
3.0	27.5	24.3	12	Very faint
1.5	26.6	25.0	6	Barely visible
0.76	27.7	25.5	8	Not visible

Table 2: Attenuators used, power readings of laser before and after it passes through dye-methanol solution of concentration 3.9 x 10^{-5} M (path length = 1 cm) and television observations of laser-induced fluorescence. The number in parentheses following each attenuator (see column 1) indicates the factor by which the attenuator reduces the intensity of the laser.

Attenuator	**Power of excitation source (mW)**	**Power of beam after passing through solution (mW)**	**Percent absorption**	**TV observations of LIF**
None	26.7	14.7	45	Fuzzy edges, 2 bright lines, fuzzy center
ND01A ($10^{0.1}$)	20.4	12.0	41	Dimmer
ND02A ($10^{0.2}$)	20.8	10.6	49	Dimmer
ND04A ($10^{0.4}$)	16.2	9.8	40	Much dimmer, no fuzzy edges, straighter line
ND05A ($10^{0.5}$)	13.7	8.9	35	Shorter, dimmer, fading at one end
ND06A ($10^{0.6}$)	12.6	9.9	21	Similar to previous
ND10A ($10^{1.0}$)	10.6	9.4	11	Barely visible at one end, very dim
ND20A ($10^{2.0}$)	9.1	8.7	4	Not visible

The glass cuvette containing the dye-methanol solutions caused much scattering of the incident light. We attempted to discriminate between scatter and laser-induced fluorescence by placing a diffraction grating between the lens and the CCD camera (see Figure 3) to separate the different wavelengths, but these attempts were unsuccessful. In order to redirect the light diffracted by the grating toward the CCD camera, we had to set up additional mirrors and lenses higher than the rest of the set up. The added height made the set up unstable, which in turn made focusing the light much more difficult.

The Avalanche Photodiode Detector

Avalanche photodiodes (APD) are high-speed, high sensitivity photodiodes capable of measuring lower intensity light than PIN photodiodes.[13] An avalanche photodiode is composed of a light absorption region and an avalanche region between its PN junction. APDs operate with

a reverse bias voltage to create internal gain. If the light entering a photodiode has more energy than the band gap energy, the incident light generates electron-hole pairs. A photodiode is sensitive to wavelengths of light less than or equal to the wavelength given by the following equation:

$$\lambda = \frac{1240}{E} \tag{1}$$

in which E is the band gap energy in eV, and ? is in nanometers. The APDs used in this experiment were silicon, whose band gap energy is 1.12 eV at room temperature. These photodiodes are therefore sensitive to radiation of wavelengths shorter than 1100 nm. The reverse bias voltage applied to the PN junction of the APD generates an electric field across the junction. When the incident light generates electron-hole pairs in the photodiode, the electrons move toward the N+ side and the holes move toward the P+ side because of this electric field. As the electric field increases, the speed at which the electron-hole pairs drift becomes saturated, and the electron-hole pairs are more likely to collide with the crystal lattice of the silicon. Electron-hole pairs that do not collide with the crystal lattice have a lot of energy. If we increase the reverse voltage, these pairs will then collide with the crystal lattice and generate additional

Figure 2-4 Gain vs. reverse voltage (S2381 to S2385)

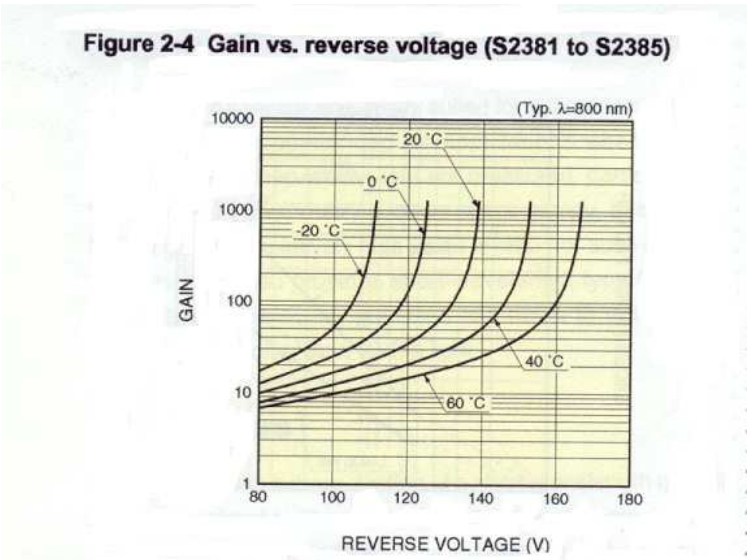

Figure 5: Plot of gain vs. reverse voltage for silicon avalanche photodiodes, taken from data sheet provided by Hamamatsu.[13] Note the rapid increase in gain as the APD approaches its breakdown voltage.

electron-hole pairs, which create more electron-hole pairs, and so on. This multiplication of the photocurrent is called an avalanche.

Measuring Gain of the Avalanche Photodiode

We used a Hewlett Packard 8082A Pulse Generator to pulse a Gigalase Vertical Cavity Surface-Emitting Laser (VCSEL). The Gigalase VCSEL operates at 850 nm, which is appropriate for our silicon APDs by Hamatsu, S2382-02 and S5139. S2382-02 and S5139 both feature stable operation at low bias voltages, high-speed response, high sensitivity at 800 nm, and low noise. The only difference between the two APDs is that S5139 has a lens covering is aperture. The pulse from the generator travels through a 33 ? resistor to the VCSEL. The signal from the laser is collimated by a lens and then reflected by a mirror to a retroreflector. The retroreflector is adjacent to a metal beam, so that its distance from the first mirror may be adjusted to add delay while maintaining the alignment of the laser beam. The beam leaving the retroreflector bounces off two more mirrors before striking the APD. We used a Kepco Power Supply to supply the reverse bias voltage of the APD (see Figure 6).

With the above set up, we measured the voltage of the output signal of the avalanche photodiode at various reverse voltages to verify that the gain increased rapidly as we approached the breakdown voltage of the APD. We initially used the S2382-02 APD in our experiment. Unfortunately, we came too close to the breakdown voltage of this APD and the APD broke down. The equally sensitive Gigalase VCSEL diode broke. This set us back a few weeks as we waited for the new equipment to arrive. We replaced the S2382-02 with a S5139 APD, which has a breakdown voltage of 139 Volts. As the data sheet for the S5139 showed (see Figure 5), the voltage of the APD signal increased very rapidly as the APD approached its breakdown

voltage (see Table 3). A 5.3 V difference in reverse voltage between 105.0 V and 110.3 V resulted in only a 12 mV difference in the amplitude of the APD signal. When we increased the reverse voltage from 125.1 V to 130.1 V, however, the difference in amplitude of the APD signal was 120 mV.

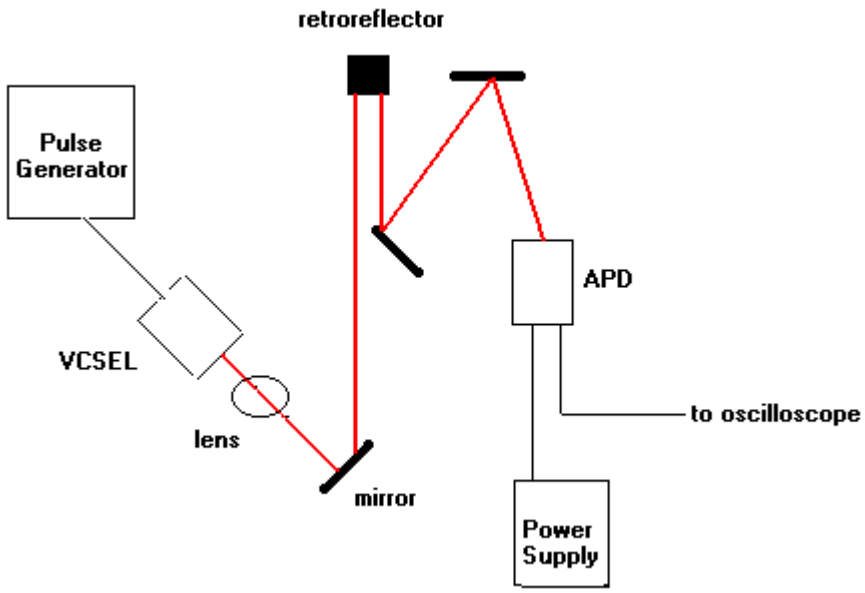

Figure 6: Set up of detection system using Gigalase VCSEL and APD. For interior of boxes labeled VCSEL and APD, see Figures 5a and 5b.

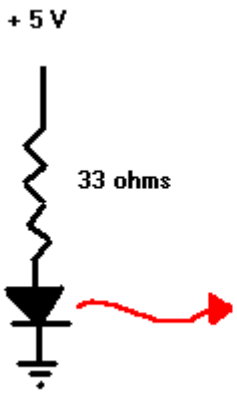

Figure 6a: Schematic of interior of VCSEL box in Figure 5.

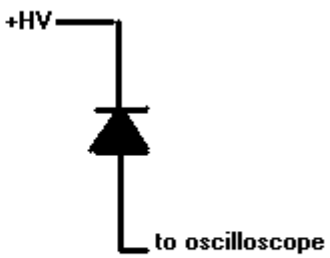

Figure 6b: Schematic of APD

Table 3: Reverse bias voltage across PN junction of APD and output signal of APD.

Reverse Voltage (V)	APD Signal Voltage (mV)
80.2	24
90.3	30
100.0	40
105.0	48
110.3	60
115.1	96
120.3	100
125.1	160
130.1	280

Modulation of the Avalanche Photodiode

To improve the gain of the APD, we modulated the bias voltage of the APD with the same modulation as the laser pulse. The signal from the pulse generator passes through a 100 pF capacitor. The capacitor allows the AC, and not the DC, signal to pass through. The voltage signal from the power supply passes through a 6.8 kΩ resistor and combines with the AC signal to give the APD a modulated bias voltage (see Figure 7).

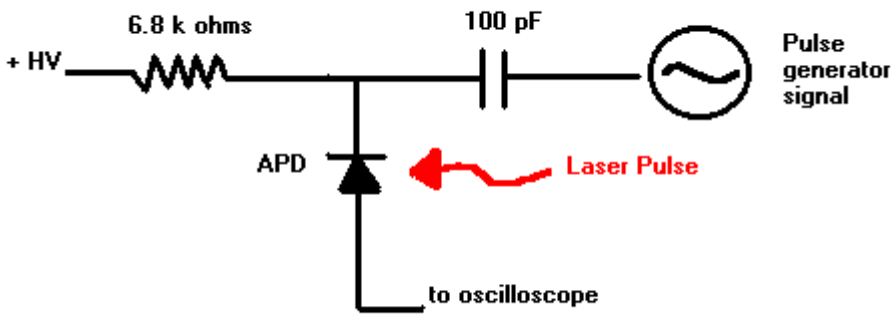

Figure 7: Reverse bias voltage passes through 6.8 kΩ resistor and signal from pulse generator passes through a 100pF capacitor (RC = 0.68 μs). These two signals combined are the new reverse bias voltage of the APD.

Table 4: Comparison of APD output signals with and without modulation at various reverse voltages

Reverse Voltage (V)	APD DC Signal (mV)	Reverse Voltage (V)	APD AC Signal (mV)	Ratio AC: DC
80.2	24	80.1	20	0.833333
90.3	30	90.1	38	1.266667
100.0	40	100.2	40	1
105.0	48	105.0	50	1.041667
110.3	60	110.0	64	1.066667
115.1	96	115.0	90	0.9375
120.3	100	120.0	124	1.24
125.1	160	125.2	200	1.25
130.1	280	130.1	440	1.571429

Adding Delay

Since the pulse generator drives both the laser and the APD, the pulse to the APD and the pulse to the laser interact. To decrease the level of interaction, we added a delay to the pulse from the generator traveling to the APD by adding a 9 m coaxial cable to the 1.5 m coaxial cable already connecting the pulse generator to the capacitor. We measured the APD output signal for a 2.2 V pulse (see Table 5) at various bias voltages.

Table 5: Comparison of APD output signal voltages for various reverse voltages, using a 2.2 V pulse, with delay

Reverse Voltage (V)	APD DC Signal (mV)	Reverse Voltage (V)	APD AC Signal (mV), with delay	Ratio AC:DC
80.2	24	80.2	16	0.67
90.3	30	90.3	44	1.47
100.0	40	100	52	1.30
105.0	48	105	68	1.42
110.3	60	110.3	84	1.40
115.1	96	115.1	100	1.04
120.3	100	120.3	160	1.60

125.1	160	125.1	270	1.69
130.1	280	130.1	400	1.43

Data Analysis

Using Kaleidograph, we fit the data for the APD DC signal versus the bias voltage to an exponential curve given by the formula

$$S = Ae^{(V/V_0)^2} \tag{2}$$

in which S is the APD signal voltage in mV, V is the bias voltage in V, and A and B are parameters equal to 1.32 mV and 3.13 x 10^{-4} V^{-2} respectively. Figure 8 shows the data points from Table 3 and the curve given by Equation 2.

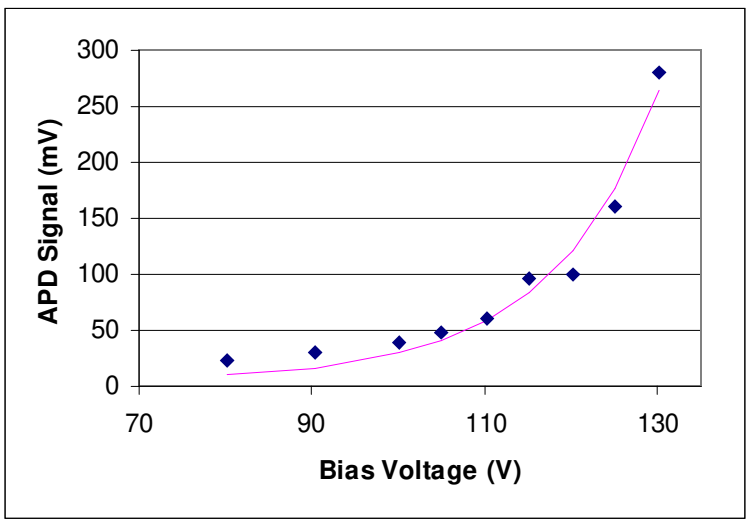

Figure 8: Plot of APD DC signal versus the bias voltage of the APD. The pink curve indicates the exponential curve given by Equation 2 and shows that the equation is a valid model for the behavior of the APD.

We assumed that the behavior of the APD with a modulated voltage could be predicted by the same equation with the following substitution:

$$V=V_{DC}+V_{AC} \quad (3)$$

in which V_{DC} is the voltage provided by the power supply and V_{AC} is the modulated voltage from the pulse generator as measured by a scope probe. For the data in Tables 4 and 5, V_{AC} was 4 V. Table 6 shows the measured and calculated APD signals for the data for the circuit with modulation and with both modulation and delay.

Table 6: Experimental and theoretical values of the modulated APD signal in mV for various bias voltages.

Modulation			Modulation and Delay		
Bias Voltage (V)	**Measured APD Signal (mV)**	**Calculated APD Signal (mV)**	**Bias Voltage (V)**	**Measured APD Signal (mV)**	**Calculated APD Signal (mV)**
80.1	20	12.1	80.2	16	12.1
90.1	38	21.1	90.3	44	21.4
100.2	40	39.6	100	52	39.0
105	50	54.5	105	68	54.5
110	64	77.3	110.3	84	79.0
115	90	111.4	115.1	100	112.2
120	124	163.0	120.3	160	166.8
125.2	200	246.3	125.1	270	244.2
130.1	440	369.0	130.1	400	368.9

Figure 9 shows the calculated and measured values of the APD signal with a modulated voltage and with a delay. The data points and calculated points are relatively close and show that our assumption (see Equation 3) is valid.

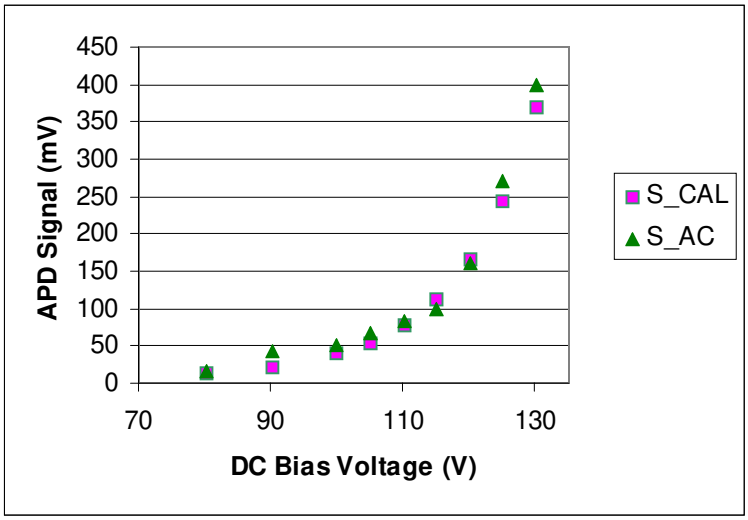

Figure 9: Comparison of the measured and calculated values for the APD AC signal, using a delayed pulse from the signal generator.

Conclusions

We have shown that by modulating the bias voltage of the APD, we can increase the gain of the APD. In some cases, we increased the gain by nearly 70% (See Table 5). Equation 3 shows us that to amplify the APD signal even more, we could modulate it with a larger pulse. To decrease the level of interaction between the pulses to the APD and to the laser, it would be best to drive each with a separate pulse generator. The next step would be to begin examining the time delay of laser-induced fluorescence to separate the scattered light from the fluorescence.

[1] Carolyn Nichol and E. Edmund Kim, "Molecular imaging and gene therapy," The Journal of Nuclear Medicine **42**, 1368-1374 (2001).
[2] Conversations with Dr. Margaret Saha, Department of Biology, College of William and Mary, 2001-2002.
[3] Ralph Weissleder, "A clearer vision for *in vivo* imaging," Nature Biotechnology **19**, 316-317 (2001).
[4] Arjun Yodh and Britton Chance, "Spectroscopy and imaging with diffusing light," Physics Today **48**, 34-40 (1995).
[5] Andreas Becker, Carsten Hessenius, Kai Licha, Bernd Ebert, Uwe Sukowski, Wolfhard Semmler, Bertram Wiedermann, and Carsgen Grotzinger, "Receptor-targeted optical imaging of tumors with near-infrared fluorescent ligands," Nature Biotechnology **19**, 327-331 (2001).
[6] Canberra Nuclear, "An introduction to time correlated single photon counting for fluorescence decay time studies," Canberra Industries, Inc.
[7] Emanuel Waddell, Yun Wang, Wieslaw Stryjewski, Scott McWhorter, Alyssa C. Henry, David Evans, Robin L. McCarley, and Steven A. Soper, "High-resolution near-infrared imaging of DNA microarrays with time-resolved acquisition of fluorescence lifetimes," Anayltical Chemistry **72**, 5907-5917 (2000).
[8] James H. Flanagan, Jr., Clyde V. Owens, Sarah E. Romero, Emanuel Waddell, Shaheer H. Kahn, Robert P. Hammer, and Steven A. Soper, "Near-infrared heavy-atom-modified fluorescent dyes for base-calling in DNA-sequencing applications using temporal discrimination," Analytical Chemistry **70**, 2676-2684 (1998).
[9] James H. Flanagan, Jr., Shaheer H. Khan, Steve Menchen, Steven A. Soper, and Robert P. Hammer, "Functionalized tricarbocyanine dyes as near-infrared fluorescent probes for biomolecules," Bioconjugate Chemistry **8**, 751-756 (1997).
[10] X. D. Li, T. Durduran, A. G. Yodh, b. Chance, and D. N. Pattanayak, "Diffraction tomography for biochemical imaging with diffuse-photon density waves," Optics Letters **22**, 573-575 (1997).
[11] R. M. Danen, Yong Wang, X. D. Li, W. S. Thayer, and A. G. Yodh, "Regional imager for low-resolution functional imaging of the brain with diffusing near-infrared light," Photochemistry and Photobiology **67**, 33-40 (1998).
[12] Brian W. Pogue and Gregory Burke, "Fiber-optic bundle design for quantitative fluorescence measurement from tissue," Applied Optics **37**, 7429-7436 (1998).
[13] Hamamatsu, "Characteristics and use of Si APD (Avalanche Photodiode)," Hamamatsu Photonics K. K., Solid State Division.